Author Manuscript

Author Manuscript

Author Manuscript

Author Manuscript

HHS Public Access

Author manuscript

Nat Neurosci. Author manuscript; available in PMC 2015 October 01.

Published in final edited form as:

Nat Neurosci. 2015 April ; 18(4): 531–535. doi:10.1038/nn.3971.

Somatostatin-expressing interneurons provide subtractive inhibition and regulate sensory response fidelity in olfactory cortex

James F. Sturgill and **Jeffry S. Isaacson**

Center for Neural Circuits and Behavior, Dept. of Neuroscience, University of California, San Diego, School of Medicine, La Jolla, CA, 92093, USA

Abstract

Diverse types of local GABAergic interneurons shape the cortical representation of sensory information. Here we show how somatostatin-expressing interneurons (SOM cells) contribute to odor coding in mouse olfactory cortex. We find that odor-tuned SOM cells regulate principal cells through a purely subtractive operation that is independent of odor identity or intensity. This operation enhances the salience of odor-evoked activity without changing cortical odor tuning. SOM cells inhibit both principal cells and fast-spiking interneurons, indicating that subtractive inhibition reflects the interplay of multiple classes of interneurons.

Introduction

Different types of interneurons play an important role in shaping cortical information processing, however, the mechanisms by which they regulate sensory coding is unclear. Inhibition is typically proposed to modulate the input-output (I-O) relationship of neurons through the arithmetic operations of subtraction or division[1,2]. Divisive inhibition, which changes the slope of the I-O relationship, provides a gain control function that regulates the amplification and normalization of activity in neural circuits. Subtractive inhibition, which causes an offset of the I-O relationship, raises the threshold for sensory input to trigger spike output: an action that can regulate the sparseness of population activity as well as response discriminability.

Recent optogenetic studies have explored the operations performed by genetically defined classes of interneuron. Indeed, channelrhodopsin-2 (ChR2) stimulation of individual interneuron populations in visual cortex alters contrast-response relationships and sensory tuning via these arithmetic functions[3–6]. However, the artificial activation of interneuron subtypes in visual cortex generated conflicting conclusions attributed to differences in the strength and timing of activation[7–9]. For example, activating interneurons beyond their

Users may view, print, copy, and download text and data-mine the content in such documents, for the purposes of academic research, subject always to the full Conditions of use:http://www.nature.com/authors/editorial_policies/license.html#terms

Correspondence: Jeffry S. Isaacson, Center for Neural Circuits & Behavior, Rm. 213, 9500 Gilman Dr. La Jolla, CA, 92093-0634, Tel: (858) 822-3525, Fax: (858) 822-4527, jisaacson@ucsd.edu.

Author Contributions: J.F.S. and J.S.I. performed experiments, analyzed data, and wrote the manuscript.

Author Manuscript Author Manuscript Author Manuscript Author Manuscript

sensory-evoked firing rates can impose threshold effects and artificially sharpen tuning[8]. In addition to these concerns, the contributions of specific interneuron populations to information coding in other sensory cortical areas is also unclear. In this study, we optogenetically suppress the endogenous activity of SOM cells to determine their contribution to odor coding in the anterior piriform cortex (PCx), a simple three layered cortical region that is critical for odor perception[10].

Results

Odor-evoked activity of optogenetically-tagged SOM cells

In PCx, somatostatin-expressing interneurons are located almost exclusively in deep layer 3[11]. As in other cortical regions, SOM cells target the dendrites of PCx layer 2/3 principal cells and provide feedback inhibition[12]. To selectively suppress SOM cells *in vivo*, we conditionally expressed the hyperpolarizing opsin Arch-GFP in the PCx of SOM-cre mice[13,14] (Supplementary Fig. 1). We recorded PCx unit activity with a multisite silicon probe[15] and activated Arch (592 nm) on interleaved trials via an LED fiber positioned over the cortical surface (Fig. 1a).

We first took advantage of the optogenetic tagging of SOM cells[16] to determine their odor tuning properties as well as our ability to suppress SOM cell activity *in vivo*. Putative SOM cells were identified as isolated single units whose firing was rapidly (<10 ms) and strongly suppressed by LED illumination (n = 11, Fig. 1b,c, Supplementary Fig. 2). SOM cells were spontaneously active (median firing rate = 3.5 Hz, range 0.4 - 30 Hz) and odor-evoked increases in activity were graded with changes in odor concentration. Importantly, LED illumination strongly and consistently suppressed SOM cell activity over a wide range of odor intensities (Fig. 1d,e, Supplementary Fig. 2). The firing of PCx principal cells is odor selective[17]; however, the odor tuning of local interneurons is unclear. Application of a panel of 11 structurally diverse monomolecular odorants revealed that SOM cells generated odor-selective responses (Fig. 1f,g) with tuning properties similar to those of principal cells (see below, Supplementary Fig. 2) and Arch photoinactivation abolished SOM cell responses to all odorants (Fig. 1f,g). Thus, SOM cells are tuned for different odors and we could reliably suppress their activity driven by different odors and stimulus intensities (Supplementary Fig. 2).

SOM cells mediate subtractive inhibition

We next examined the effects of SOM cell suppression on principal neurons, the most numerous cells in layer 2/3 that contribute the majority of extracellular responses. We recorded multiunit activity (Fig. 2a) while varying the concentration of a single odorant (amyl acetate) to determine how SOM cells regulate the odor intensity-response relationship in PCx. LED inactivation of SOM cells caused sustained increases in spontaneous multiunit activity (165 ± 12%, n = 11, Fig. 2b), indicating that SOM cells normally dampen basal firing rates in PCx. Remarkably, photoinactivation of SOM cells uniformly enhanced responses in the presence of odor regardless of odor intensity. In other words, odor responses during SOM cell suppression were simply increased by the spikes added to the spontaneous firing rate. To quantify the effect of SOM cell inactivation, we plotted firing

Author Manuscript Author Manuscript Author Manuscript Author Manuscript

rates in the presence of the different odor concentrations for the LED off vs. the LED on condition (Fig. 2c). The data were well described by a linear function (r = 0.94 ± 0.06, n = 11 experiments, Fig. 2d) with slopes (*m*) that were not different from unity (*m* = 1.03 ± 0.05) but with *y*-intercepts (*b*) significantly offset from zero (*b* = 21.3 ± 4.3, p<0.005). Identical results were obtained from analyses of single unit activity (321 ± 43% increase in spontaneous firing rate, *m* = 1.12 ± 0.08, *b* = 1.02 ± 0.30, p<0.001, n = 21 units, Supplementary Fig. 3). The offset *y*-intercept and unity slope of this response function shows that suppressing SOM cells caused a completely additive, linear transformation of PCx activity. Indeed, the pure vertical shift of the odor intensity-response curve (Fig. 2e) indicates that this form of subtractive inhibition is effectively independent of sensory input[1].

SOM cells regulate sensory response fidelity without altering odor tuning

If SOM cell-mediated inhibition is purely subtractive, how does suppressing SOM cells affect the odor tuning properties of PCx principal cells? We addressed this question by studying the responses of individual layer 2/3 cells (Arch-negative single units) to 11 concentration-matched odorants (100 ppm). Odor-tuned firing of layer 2/3 cells was enhanced by SOM cell photoinactivation; however, the increase in firing during LED trials was unrelated to the strength of the control odor response (Fig. 3a). Responses to the different odorants for the LED on vs. LED off condition were well fit by lines with a significant offset but a slope not different from unity (Fig. 3b,c, slope = 1.09 ± 0.05, *y*-intercept = 1.46 ± 0.23, p<0.001, n=29 units). These findings indicate that SOM cell-mediated inhibition acts entirely through a subtractive mechanism that is independent of the identity of the odorant driving PCx activity. Indeed, LED photoinactivation caused a uniform, vertical shift in normalized firing rate curves derived from rank-ordering responses of layer 2/3 cells activated by the different odorants (Fig. 3d, n=18 units). However, the odor-evoked component of responses, derived by subtracting the spontaneous firing rate during LED trials, reveals that the odor tuning of PCx cells is entirely unaffected (Fig. 3d).

Although odor-evoked firing and tuning are unaltered when SOM cells are suppressed, SOM cell-mediated inhibition should improve the fidelity of sensory responses by reducing variability associated with stimulus-independent (“background”) cortical activity. To test this idea we computed the discriminability index (d', Methods), an estimate of response reliability from signal detection theory[18,19], with and without SOM cell photoinactivation (Fig. 3e). Suppressing SOM cells significantly reduced the discriminability of odor-evoked activity ($d'_{\text{LED off}}$ = 2.01 ± 0.17; $d'_{\text{LED on}}$ = 1.64 ± 0.18, n=18, p <0.05) indicating that SOM cell inhibition normally serves to enhance the representation of odor responses relative to spontaneous activity in PCx.

SOM cells modulate other interneurons in PCx

What accounts for the lack of effect of SOM cell suppression on odor-evoked principal cell activity? In neocortex, SOM cells inhibit other interneuron subtypes, but not themselves[20]. This raises the possibility that decreases in SOM cell activity could disinhibit other interneuron types that provide compensatory inhibition onto pyramidal cells. We therefore examined the relative impact of SOM cells on local fast-spiking (FS) cells; a different class of PCx interneurons that express parvalbumin (PV) and/or calbindin and mediate somatic

Author Manuscript Author Manuscript Author Manuscript Author Manuscript

feedback inhibition[12,21,22]. We made in vitro whole-cell recordings from layer 2/3 pyramidal (Pyr) and FS cells in PCx slices from mice that conditionally expressed ChR2 in SOM cells (Fig. 4a,b). Pyr cells were identified by their morphology and firing properties in response to threshold current injection (initial burst of action potentials (APs) and prominent firing rate adaptation). In the same slices, we recorded from nearby (within 200 μm) FS cells distinguished by their multipolar morphology, lack of firing rate adaptation, and faster AP waveforms (AP width at half-maximum: Pyr = 1.8 ± 0.1 ms, FS = 1.2 ± 02 ms, p=0.03, paired t-test, n=7 cell pairs)[12,21,22]. In voltage clamp, photoactivation of ChR2-expressing SOM cells evoked inhibitory postsynaptic currents (IPSCs) onto both Pyr and FS cells (Fig. 4b,c, average conductance: Pyr = 8.0 ± 2.3 nS and FS = 6.2 ± 0.9 nS, p=0.45, paired t-test, n=7 cell pairs). These results suggest that the suppression of SOM cell activity in vivo could disinhibit FS cells and enhance FS cell-mediated inhibition of principal cells.

To further explore the interactions between these interneurons, we examined the effect of SOM cell photoinactivation on FS units isolated from our in vivo recordings (Fig. 4d). Intriguingly, unlike the simple addition of spikes we observed for regular spiking units, SOM cell suppression added spikes but also enhanced FS unit activity in proportion to the magnitude of the odor-evoked response (Fig. 4e,f). Responses of FS units to odors for the LED off vs. LED on condition were well fitted by lines with a slope significantly greater than unity (Fig. 4g, $p<0.05$, $m = 1.44 \pm 0.18$, $b = 3.22 \pm 0.99$, n = 12 units). This indicates that SOM cell suppression leads to a multiplicative increase in FS cell activity, which in turn can provide compensatory odor-evoked inhibition onto PCx principal cells. Using the conditional expression of ChR2 in PV-Cre mice, we also explored how increasing FS cell activity modulates the odor intensity-response relationship of regular spiking units (Supplementary Fig. 4). PV cell activation caused a larger suppression of activity when control responses were higher, consistent with previous studies reporting that PV cells mediate divisive inhibition[3,5]. Taking the simplest interpretation, this divisive action by FS/PV cells could provide an additional means of compensating for changes in SOM-cell inhibition. Thus, we think it likely that the purely subtractive action of SOM cells on PCx principal cells reflects mechanisms involving both direct and indirect inhibitory circuits (Fig. 4h).

Discussion

We show that SOM cells exert subtractive inhibition of principal cells in olfactory cortex. This computation subtracts the same of number of spikes in individual principal cells regardless of their sensory-evoked activity. Thus, SOM cell-mediated inhibition reduces spontaneous and odor-evoked activity equally such that principal cell odor tuning is unaltered. Our results reveal that the mechanism underlying this computation may arise from the fact that SOM cells directly inhibit other local interneurons that also mediate feedback inhibition. Finally, we show that an important consequence of subtractive SOM cell inhibition is the regulation of response discriminability.

Previous optogenetic studies in visual cortex have suggested several roles for SOM cells in sensory information processing. Photoinactivation of SOM cells indicated that this class of interneurons contributes to a cortical circuit for surround suppression[23]. Activation of SOM

Author Manuscript Author Manuscript Author Manuscript Author Manuscript

cells has also been shown to elicit subtractive inhibition of principal cell contrast-response functions, with strong shifts in response levels leading to the sharpening of stimulus selectivity[3]. In contrast, rather than acting via subtraction it has also been reported that ChR2 activation of SOM cells elicits divisive inhibition, thus providing gain control that does not alter tuning properties[4]. These discrepancies were recently argued[7,9] to depend on differences in the magnitude and temporal patterns of stimulation or the fact that SOM cells also inhibit fast-spiking PV cells[6,20,24] in neocortex. Regardless of these studies using ChR2 activation in visual cortex, our findings using optogenetic photosuppression clearly indicate that SOM cells mediate subtractive inhibition in olfactory cortex.

We show that SOM cells inhibit both principal cells and FS cells in olfactory cortex. These results are consistent with findings that SOM cells inhibit PV cells and other interneuron subtypes in primary visual cortex [20]. Thus, any changes in SOM cell activity have direct effects on the excitability of principal cells as well as indirect effects due to the regulation of FS cell-mediated inhibition. Indeed, we find that suppressing SOM cells leads to a multiplicative increase in FS cell activity that could compensate for the reduction in the direct SOM cell inhibition of principal cells. While compensatory changes in the recruitment of FS cells provide a potential mechanism for the subtractive effects of SOM cells on principal cell activity, we do not exclude the possibility that more complex circuit mechanisms and network effects also contribute.

What is the significance of subtractive inhibition in olfactory cortex? Odor representations in PCx reflect the sparse activity of overlapping and dispersed ensembles of pyramidal cells[17,25]. Given that subtractive inhibition is ideal for regulating response thresholds, SOM cells may play an important role in enforcing a sparse population coding strategy. We also show that SOM cells normally act to maintain low spontaneous firing rates without altering odor tuning. This operation could govern the salience of odors encoded in olfactory cortex (and perhaps perceptual acuity) by regulating the ability to discriminate odor responses from background cortical activity.

Methods

Viral Injections of SOM-cre and PV-cre Mice

Experiments followed approved national and institutional guidelines for animal use. High-titer ($\sim 2*10^{12}$) stocks of AAV-2/9-CBA-Flexed-Arch-GFP and AAV-2/9-EF1a.DIO.hChR2(H134R)-eYFP.WPRE.hGH were obtained from the U. Penn. Vector Core. Mice were maintained at an institutional facility on a normal light/dark cycle with no more than 5 mice/cage. Animals were used only for the described experiments prior to euthanization. Neonatal (postnatal day 1-3) SOM-IRES-Cre mice (JAX 013044) or PV-cre mice (JAX 008069) were anesthetized and virus injection sites targeting the anterior PCx were determined based on landmarks including the superficial temporal vein and the posterior border of the eye. Injections (23 nl) were made using beveled pipettes (Nanoject II, Drummond) at 4 injection sites at depths of 0.18-0.25 mm.

Author Manuscript Author Manuscript Author Manuscript Author Manuscript

Immunohistochemistry

Under urethane anesthesia, animals (n=3) were transcardially perfused with 4% paraformaldehyde in PBS, and the brain rapidly extracted. Coronal sections (50 μm) were cut, blocked in a solution of 4% normal goat serum (NGS) and incubated overnight with an anti-somatostatin antibody previously validated by indirect immunofluorescence labeling of hypothalamic sections (Immunostar, rabbit) at a dilution of 1:500. Slices were subsequently washed in PBS, incubated for 2 hr with an Alexa-594 conjugated goat anti-rabbit secondary antibody (Life Technologies) at a concentration of 1:500, and washed a second time. After mounting (Vectashield mounting medium with DAPI) and imaging (Zeiss Axio Imager), Arch-expressing somata were first identified, blind to somatostatin immunoreactivity, and thereafter scored for colocalization.

In separate immunohistochemical experiments we detected negligible overlap between cre-expressing somatostatin cells and cells expressing parvalbumin (data not shown). Although we cannot exclude the possibility that some SOM-cre neurons express markers of other interneuron subtypes, the most parsimonious explanation for our results using SOM-cre mice is that we are predominantly manipulating SOM cells.

In Vivo Recording

Virally injected animals between 2 and 6 months of age, without regard for gender, were anesthetized with urethane (1.5 g/kg) and chlorprothixene (2 mg/kg) and maintained at a body temperature of 35-37°C. Piriform cortex was surgically exposed and a craniotomy anterior to the medial cerebral artery and just dorsal to the lateral olfactory tract was opened for insertion of a 16-channel silicon probe (Neuronexus, A1x16-Poly2-5mm-50s-177-A16 or A1x16-5mm-25-177-A16). Penetration depths were between 500-700 μm and placement in PCx was confirmed in a subset of experiments by painting the recording probe with a fluorescent DiI solution (Life Technologies, Vybrant DiI solution). A fiber-coupled LED (592 nm, 10 mW, 1mm fiber, 0.48 N.A. or 470 nm, 20 mW, 1 mm fiber, 0.48 N.A., Doric Lenses) was positioned 1-2 mm superficial to the cortical surface for optogenetic manipulations. For PV cell activation experiments, the LED intensity was set to achieve a moderate (∼30-50%) suppression of spontaneous, multiunit activity.

Odors were delivered at a flow rate of 1 L/min via a computer-controlled olfactometer and diluted in mineral oil to achieve a final concentration at the animals' snout of 100 ppm unless otherwise stated. For each odor, this fixed concentration was achieved by 1) calculating the molar ratio of odorant vs. air for the pure odorant according to the ideal gas law (PV=nRT) using the characteristic vapor pressure of each odorant (http://www.thegoodscentscompany.com) and assuming equilibrium under standard conditions within the headspace of odor-containing vials and 2) diluting proportionately with mineral oil. Odorants were: octanol, limonene, cis-3-hexen-1-ol, cineole, ethyl tiglate, octanal, hexanal, heptaldehyde, amyl acetate, cumene, 2-heptanone and anisole. For odor presentations, airflow was diverted from an empty vial to an odor vial using 2-way solenoid valves, PFTE tubing and manifolds (NResearch). A check valve was placed after each vial to prevent backflow and odor cross-contamination. Respiration was monitored with a

Author Manuscript Author Manuscript Author Manuscript Author Manuscript

thermocouple placed in front of the ipsilateral naris to confirm regular and unimpeded breathing.

Unit activity was recorded with a 16-channel amplifier (AM systems) at 20 kHz. Data were digitized (National Instruments) and acquired with custom software in Matlab that was also used to trigger the olfactometer and LED. Odor and LED trials were presented in pseudorandomized order every 30 s. Between 10 and 20 trials were acquired per experimental condition in order to sensitively detect modulation of firing rates by odorants and LED illumination.

Brain slice experiments

For SOM cell photoactivation, we used mice that were heterozygous for SOM-IRES-Cre and Rosa-LSL-ChR2 (Allen Institute line Ai32, Jackson Labs no. 012569). Mice (2-3 weeks old) were anesthetized with isoflurane and decapitated. Brains were removed and placed into ice cold artificial cerebrospinal fluid (aCSF) containing (in mM) 83 NaCl, 2.5 KCl_2, 0.5 $CaCl_2$, 3.3 $MgSO_4$, 1 NaH_2PO_4, 26.2 $NaHCO_3$, 22 glucose, and 72 sucrose, equilibrated with 95% O_2 and 5% CO_2. Coronal slices (300- 400 μm thickness) containing the anterior PCx were cut using a vibrating slicer and incubated at 35° C for 30 minutes. Slices were transferred to a recording chamber and superfused with aCSF containing (in mM): 119 NaCl, 5 KCl, 2.5 $CaCl_2$, 1.3 $MgSO_4$, 1 NaH_2PO_4, 26.2 $NaHCO_3$ and 22 glucose, equilibrated with 95% O_2 and 5% CO_2. All experiments were conducted at 28–30° C.

Patch-clamp recordings were performed using an upright microscope and DIC optics. Recordings were made using a Multiclamp 700A amplifier (Molecular Devices) digitized at 20 kHz and acquired using AxographX software. For most current and voltage-clamp recordings, pipettes (3-6 MΩ) contained (in mM: 150 Kgluconate, 1.5 $MgCl_2$, 5 HEPES buffer, 0.1 EGTA 10 phosphocreatine, and 2.0 Mg-ATP [pH 7.4], Chloride reversal potential ≈-80 mV). In some experiments, the internal solution contained KCl in place of Kgluconate. Series resistance was routinely <20 MΩ and continuously monitored. Output from a xenon lamp (470 nm, TILL) was directed through the 40× microscope objective for full-field photoactivation of ChR2.

In vivo Data Analysis and Statistics

Data analysis was performed using a custom Matlab program that incorporates an open-source, K-means clustering algorithm and spike-sorting graphical user interface (UltraMegaSort2000, Hill and Kleinfeld). Data were preprocessed by digitally filtering between 0.3 and 8 kHz using a 5^{th} order Butterworth filter. Spike sorting was conducted blind to experimental outcome and single units with >40% estimated spike contamination were excluded. LED-enhanced regular spiking (RS) units were identified by comparing control and LED firing rates during the 2 s period of odor valve activation and based upon the following empirically determined criteria: 1) significant change in firing rate ($p<0.05$, paired T-test), 2) a z-score > 0.5, and 3) spike width > 0.5 ms. Only units with linearly correlated firing (Pearson's $R > 0.5$) for control and LED conditions were included in analysis to determine slope and intercept changes. Units lacking linearly correlated firing typically lacked substantial odor responses and/or exhibited high response variability

Author Manuscript Author Manuscript Author Manuscript Author Manuscript

precluding further analysis. Individual unit linear fits and confidence intervals for slope and intercept were generated using the Matlab curve fitting toolbox and a 1st order polynomial model. To generate odor intensity-response curves, firing rates were first baselined by subtraction of the control, spontaneous firing rate (FR) and then normalized by the control FR in the presence of maximal odorant concentration (500 ppm). For odor tuning curves, the same baseline subtraction and normalization procedure was conducted except the FR associated with the most preferred odor for a given unit was used for the normalization step. The discriminability index, d′, was calculated for every LED-enhanced, odor-unit pair as $(\text{mean } FR_{odor} - \text{mean } FR_{spontaneous}) / \sqrt{(0.5 * (\sigma^2_{odor} + \sigma^2_{spontaneous}))}$[19]. Odor-unit pairs were excluded if their odor vs. spontaneous FR z-score was <2. The d′ values for all odor responses for an individual unit were averaged. Average LED modulation values were derived from every odor condition for a given unit and calculated as $(FR_{LED} - FR_{ctl}) / (FR_{LED} + FR_{ctl})$. SOM cells were defined by a LED modulation score < -0.2. For the SOM population, the median LED modulation value was -0.73.

For the isolation of fast spiking (FS) units, average spike waveforms were first generated for each single unit from a randomly selected subset of 300 identified spikes. Next, spike width was calculated from this average as the latency between the initial trough and subsequent peak[26]. FS units were defined from the tail of this distribution as those units with a trough to peak latency below 0.4 ms. Consistent with disinhibition by SOM cell photoinactivation, the median LED modulation value for all FS units was 0.24 ($p<0.05$, $n=15$). In order to determine how the odor responses of FS units are scaled by SOM cell photoinactivation, the same criteria previously used to identify odor-modulated RS units was applied to the FS population: 1) significant LED-enhancement of firing rate ($p<0.05$, paired T-test), 2) z-score for LED effect > 0.5, and 3) Pearson's linear correlation coefficient > 0.5.

Unless otherwise stated, all statistical comparisons were performed using a 2-tailed Wilcoxon Signed-Rank test, a non-parametric test appropriate for the presented data as it makes no assumptions of normality. In figures, error bars correspond to +/- the standard error of the mean (SEM) unless otherwise stated.

Supplementary Material

Refer to Web version on PubMed Central for supplementary material.

Acknowledgments

We thank M. Scanziani, K. Franks, P. Frady and members of the Isaacson and Scanziani labs for advice and helpful discussions. Supported by the NIDCD (R01DC04682, J.S.I.; 5F32DC013511, J.F.S.).

References

1. Silver RA. Neuronal arithmetic. Nat Rev Neurosci. 2010; 11:474–89. [PubMed: 20531421]
2. Isaacson JS, Scanziani M. How inhibition shapes cortical activity. Neuron. 2011; 72:231–43. [PubMed: 22017986]
3. Wilson NR, Runyan CA, Wang FL, Sur M. Division and subtraction by distinct cortical inhibitory networks in vivo. Nature. 2012; 488:343–8. [PubMed: 22878717]

Author Manuscript Author Manuscript Author Manuscript Author Manuscript

4. Lee SH, et al. Activation of specific interneurons improves V1 feature selectivity and visual perception. Nature. 2012; 488:379–83. [PubMed: 22878719]
5. Atallah BV, Bruns W, Carandini M, Scanziani M. Parvalbumin-expressing interneurons linearly transform cortical responses to visual stimuli. Neuron. 2012; 73:159–70. [PubMed: 22243754]
6. Cottam JCH, Smith SL, Häusser M. Target-specific effects of somatostatin-expressing interneurons on neocortical visual processing. J Neurosci. 2013; 33:19567–78. [PubMed: 24336721]
7. Lee SH, Kwan AC, Dan Y. Interneuron subtypes and orientation tuning. Nature. 2014; 508:E1–2. [PubMed: 24695313]
8. Atallah BV, Scanziani M, Carandini M. Atallah et al. reply. Nature. 2014; 508:E3. [PubMed: 24695314]
9. El-Boustani S, Wilson NR, Runyan CA, Sur M. El-Boustani et al. reply. Nature. 2014; 508:E3–4. [PubMed: 24695315]
10. Wilson DA, Sullivan RM. Cortical processing of odor objects. Neuron. 2011; 72:506–19. [PubMed: 22099455]
11. Suzuki N, Bekkers JM. Inhibitory neurons in the anterior piriform cortex of the mouse: classification using molecular markers. J Comp Neurol. 2010; 518:1670–87. [PubMed: 20235162]
12. Suzuki N, Bekkers JM. Distinctive classes of GABAergic interneurons provide layer-specific phasic inhibition in the anterior piriform cortex. Cereb Cortex. 2010; 20:2971–84. [PubMed: 20457693]
13. Chow BY, et al. High-performance genetically targetable optical neural silencing by light-driven proton pumps. Nature. 2010; 463:98–102. [PubMed: 20054397]
14. Taniguchi H, et al. A resource of Cre driver lines for genetic targeting of GABAergic neurons in cerebral cortex. Neuron. 2011; 71:995–1013. [PubMed: 21943598]
15. Boyd AM, Sturgill JF, Poo C, Isaacson JS. Cortical feedback control of olfactory bulb circuits. Neuron. 2012; 76:1161–74. [PubMed: 23259951]
16. Royer S, et al. Control of timing, rate and bursts of hippocampal place cells by dendritic and somatic inhibition. Nat Neurosci. 2012; 15:769–75. [PubMed: 22446878]
17. Poo C, Isaacson JS. Odor representations in olfactory cortex: “sparse” coding, global inhibition, and oscillations. Neuron. 2009; 62:850–61. [PubMed: 19555653]
18. Tolhurst DJ, Movshon JA, Dean AF. The statistical reliability of signals in single neurons in cat and monkey visual cortex. Vision Res. 1983; 23:775–85. [PubMed: 6623937]
19. Duguid I, Branco T, London M, Chadderton P, Häusser M. Tonic inhibition enhances fidelity of sensory information transmission in the cerebellar cortex. J Neurosci. 2012; 32:11132–43. [PubMed: 22875944]
20. Pfeffer CK, Xue M, He M, Huang ZJ, Scanziani M. Inhibition of inhibition in visual cortex: the logic of connections between molecularly distinct interneurons. Nat Neurosci. 2013; 16:1068–76. [PubMed: 23817549]
21. Stokes CCA, Isaacson JS. From dendrite to soma: dynamic routing of inhibition by complementary interneuron microcircuits in olfactory cortex. Neuron. 2010; 67:452–65. [PubMed: 20696382]
22. Suzuki N, Bekkers JM. Microcircuits mediating feedforward and feedback synaptic inhibition in the piriform cortex. J Neurosci. 2012; 32:919–31. [PubMed: 22262890]
23. Adesnik H, Bruns W, Taniguchi H, Huang ZJ, Scanziani M. A neural circuit for spatial summation in visual cortex. Nature. 2012; 490:226–31. [PubMed: 23060193]
24. Xu H, Jeong HY, Tremblay R, Rudy B. Neocortical somatostatin-expressing GABAergic interneurons disinhibit the thalamorecipient layer 4. Neuron. 2013; 77:155–67. [PubMed: 23312523]
25. Stettler DD, Axel R. Representations of odor in the piriform cortex. Neuron. 2009; 63:854–64. [PubMed: 19778513]
26. Bortone DS, Olsen SR, Scanziani M. Translaminar inhibitory cells recruited by layer 6 corticothalamic neurons suppress visual cortex. Neuron. 2014; 82:474–85. [PubMed: 24656931]

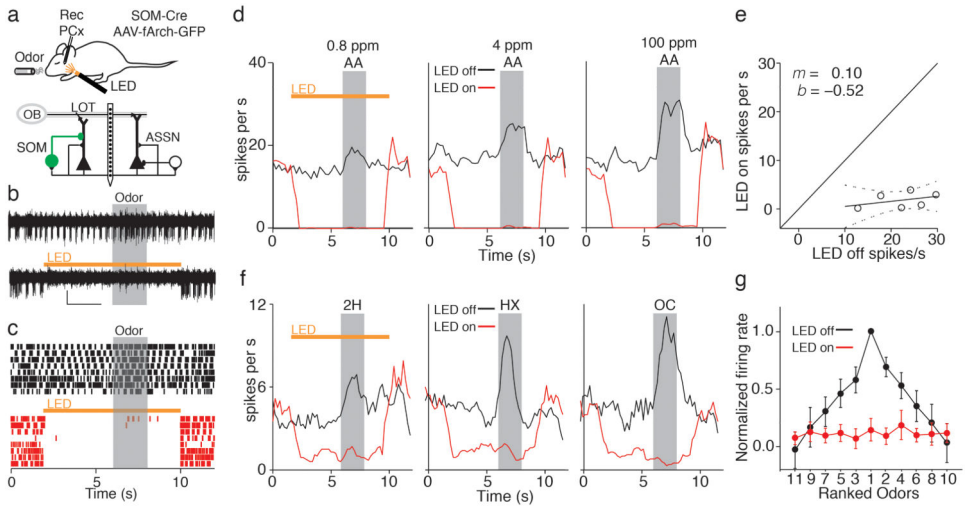

Figure 1. Optogenetic suppression of piriform cortex SOM cells

a) Top, Experimental setup. Bottom, circuit diagram: layer 2/3 principal cells receive olfactory bulb (OB) input via the lateral olfactory tract (LOT) and associational (ASSN) excitation. Principal cells receive inhibition from SOM cells expressing Arch-GFP (green) and other interneurons (white). **b)** Representative recording of a putative SOM cell unit under control conditions (top) and during LED illumination (bottom, orange bar). Grey box indicates odor delivery. Scale bar: 10 μV, 2 s. **c)** Raster plot of SOM cell activity during control trials (black) and interleaved trials with LED illumination (red). d) Peristimulus time histograms (PSTHs) of a SOM unit show responses graded with odorant concentration (black) and consistent suppression during LED illumination (red). AA; amyl acetate. e) Responses of the same cell to six concentrations of odorant (0, 0.8, 4, 20, 100, and 500 ppm) and linear fit ($y = mx + b$, $m = 0.1$, $b = –0.5$, dashes= 95% confidence interval). **f)** SOM cell activity is odor selective and uniformly blocked using Arch. Responses of a SOM cell to three different odorants under control conditions (black) and during LED illumination (red). 2H; 2-heptanone, HX; hexanal, OC; octanol. **g)** Summary data (n = 4 cells, mean ± SEM) of normalized and rank-ordered odor responses during LED off (black) and LED on (red) conditions.

Author Manuscript Author Manuscript Author Manuscript Author Manuscript

Author Manuscript Author Manuscript Author Manuscript Author Manuscript

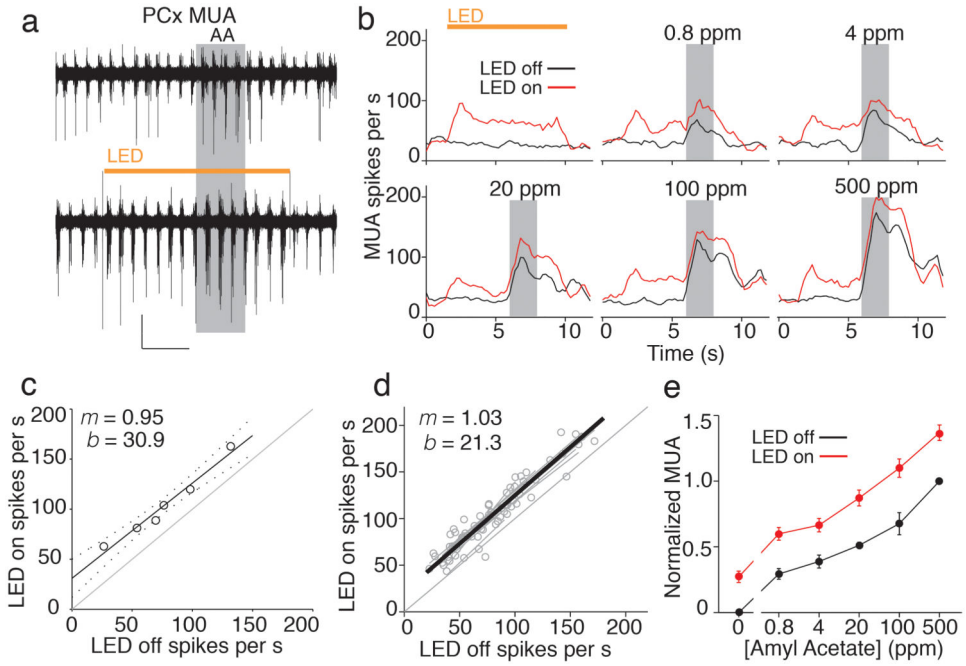

Figure 2. SOM cells provide subtractive inhibition in piriform cortex

a) PCx multiunit activity (MUA) is enhanced by SOM cell photoinactivation. Traces show interleaved trials with LED off (top) and LED on (bottom, orange bar) from a representative recording. AA; amyl acetate. **b)** Individual experiment showing effects of SOM cell inactivation on MUA evoked by different concentrations of amyl acetate (grey boxes). **c)** Line fit to MUA for six odor intensities in **b** shows that LED illumination leads to a significant offset in intercept (*b*) without altering slope (*m*) of PCx activity. **d)** Summary of 11 experiments (grey points and lines) and average of the linear fits (thick black line) shows a purely additive shift in PCx activity. **e)** Normalized odor intensity-response curves (n=11, mean ± SEM) for MUA under control conditions (black) and during SOM cell inactivation (red). The increase in activity caused by the LED at 0 ppm distinguishes a vertical from horizontal shift of the odor intensity-response curve.

Author Manuscript Author Manuscript Author Manuscript Author Manuscript

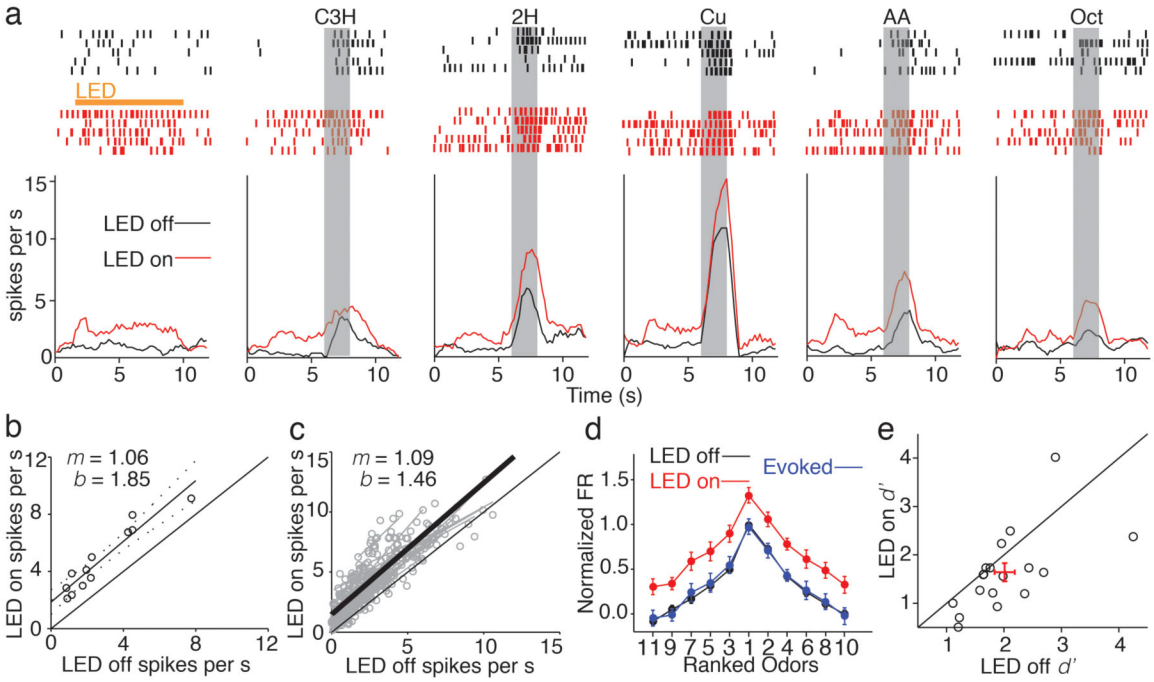

Figure 3. Subtractive inhibition increases the discriminability of odor responses without altering odor tuning in piriform cortex

a) Example single unit shows odor-tuned responses under control conditions (black) and during SOM cell photoinactivation (red). **b)** Linear fit of unit in A in response to 11 odorants with and without LED illumination reveals a significant shift in intercept (b) while slope (m) remains near unity. **c)** Summary of 29 units from 8 experiments (grey points and lines) and average of the linear fits (thick black line) shows purely additive shift in PCx activity. **d)** Average normalized and rank ordered odor tuning curve (n = 29, mean ± SEM). Control (black) and LED (red) curves are scaled by subtracting the control spontaneous firing rate and then dividing by the control peak odor response for each unit. To calculate odor-evoked activity, LED odor responses were baselined by subtracting the LED spontaneous firing rate and then normalized by the maximum LED response (blue). **e)** Discriminability index (d') is reduced during LED illumination indicating that suppressing SOM cell activity degrades the signal-to-noise ratio of odor responsive single units in PCx. Red cross; mean ± SEM.

Author Manuscript
Author Manuscript
Author Manuscript
Author Manuscript

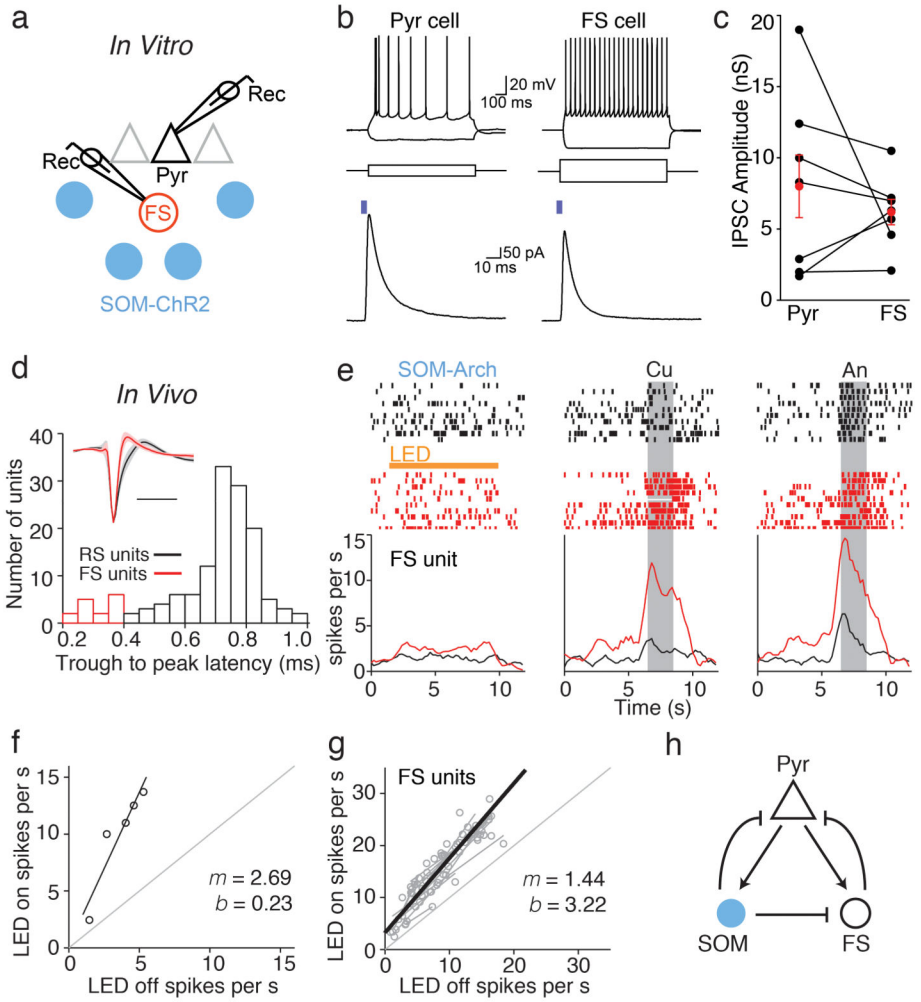

Figure 4. SOM cell suppression leads to the disinhibition of FS local interneurons

a) Recording schematic for in vitro brain slice experiments. Whole cell recordings from pyramidal neurons (triangle) and nearby fast spiking (FS) cells (red circle) were used to measure IPSCs evoked by LED stimulation of ChR2-expressing SOM cells (blue circles). **b)** Top, membrane potential responses of a pyramidal (Pyr) cell (left) and FS cell (right) to depolarizing and hyperpolarizing current steps (middle). Bottom, LED illumination (blue bar, 4 ms, 470 nm) elicits IPSCs in the same cells recorded in voltage clamp (-50 mV). **c)** Summary of ChR2-evoked inhibitory conductances. Lines, individual Pyr-FS pairs; red circles, mean ± SEM. **d)** Isolation of FS units from in vivo recordings by waveform analysis. Histogram of trough to peak latency values with FS units indicated in red. Inset, average spike waveforms (solid lines) of RS and FS units. Shaded regions correspond to ± 1 standard deviation. **e)** Raster plots (top) and trial histograms (bottom) for control (black) and SOM cell photoinactivation (red) trials for a representative FS unit in the absence of odor (left) and in response to cumene (Cu) and anisole (An). **f)** Linear fit of the example unit in **e**. **g)** Summary of 12 FS units from 9 experiments (grey points and lines) and average of the linear fits (thick black line) demonstrating multiplicative scaling (slope $m > 1$) of FS firing rates across odorants. **h)** Inhibitory circuit schematic: optogenetic suppression of SOM cells

(blue) causes both a direct reduction in the inhibition of Pyr cells (black triangle) as well as an indirect increase in inhibition mediated by FS cells (black circle).

Author Manuscript Author Manuscript Author Manuscript Author Manuscript